Modeling of Liquid Jets Injected Transversely into a Supersonic Crossflow

S. D. Heister,* T. T. Nguyen,* and A. R. Karagozian†
University of California, Los Angeles, California

This paper describes analytical/numerical modeling of a single nonreacting liquid jet in compressible (high subsonic and supersonic) crossflows. Inviscid, compressible flow about the elliptical cross section of the jet is solved numerically, using a procedure based on that of Godunov. An external boundary-layer analysis along the surface of the ellipse allows determination of a local drag coefficient associated with the jet cross section, which balances centripetal forces resulting from jet deflection. Mass and momentum balances performed along the jet, with and without the inclusion of mass loss due to droplet shedding, are then incorporated so that liquid jet penetration and bow shock shape may be calculated. Comparisons of these predictions are made with experimental results.

Nomenclature

A = cross-sectional area of elliptical recirculation cell
C_D = drag coefficient
h = vortex pair half-spacing
m = mass of liquid contained in jet cross section
$\dot{m}$ = rate at which mass is lost from jet per unit depth
M_o = local Mach number outside of external boundary layer
M_∞ = freestream Mach number
P = pressure
(PSI,ETA) = transformed variables representing ellipse
R^2 = jet-to-crossflow momentum flux ratio, $R^2 \equiv \rho_j U_j^2/\rho_\infty U_\infty^2$
Re_∞ = Reynolds number $\equiv U_\infty h/\nu_\infty$
s = distance along jet trajectory
u_i = velocity within internal boundary layer
U_i = velocity at edge of internal boundary layer
u_j = average axial velocity within jet
U_j = velocity of jet at orifice
u_{o1}, u_{o2} = velocity within external boundary layer (u_{o1} corresponds to fourth-order polynomial; u_{o2} corresponds to fifth-order polynomial)
U_o = velocity outside external boundary layer
U_s = velocity at liquid-gas surface
U_∞ = freestream velocity
x = distance along elliptical surface
(X,Y) = physical variables representing ellipse
x_s = location of external boundary-layer separation
x/d, z/d = spatial variables describing jet trajectory (nondimensionalized by orifice diameter)
Γ_i = effective dimensionless circulation of internal (liquid) flow
Γ_s = effective dimensionless circulation of surface flow
δ = external boundary-layer thickness
δ_i = internal boundary-layer thickness
$\lambda, \lambda_1, \lambda_2$ = dimensionless boundary-layer parameters
ν_o = kinematic viscosity outside of external boundary layer
ν_∞ = kinematic viscosity of freestream gas
ρ = density
ρ_i = density of liquid
ρ_o = density outside of external boundary layer
ρ_s = density of gas at liquid-gas interface
τ_s = wall (surface) shear stress
ϕ = angle of orientation of jet cross section

Presented as Paper 88-0100 at the 26th Aerospace Sciences Meeting, Reno, NV, Jan. 11-14, 1988; received March 30, 1988; revision received Oct. 15, 1988.

*Graduate Research Assistant.
†Associate Professor, Department of Mechanical, Aerospace and Nuclear Engineering. Member AIAA.

Introduction and Background

THE recent resurgence of interest in hypersonic vehicles incorporating the Supersonic Combustion Ramjet (SCRAMJET) engine has led to a renewed effort in developing an understanding of supersonic combustion processes. One of the fuel-injection schemes currently under consideration consists of introducing a fuel jet (either in the liquid or gaseous phase) transversely into the supersonic crossflow of air entering the SCRAMJET combustor.[1,2] To effectively implement this injection scheme, an understanding of transverse jet mixing and behavior for a considerable range of compressible crossflow regimes is required. The present study focuses on the problem of the liquid jet in supersonic (and high subsonic) crossflows, and describes an analytical/numerical model developed at UCLA that predicts jet behavior in this environment.

In the 1960's, interest in transverse jet injection arose primarily from technical applications dealing with rocket thrust vector control and with the control of hypersonic re-entry vehicles. Both reacting and nonreacting jets were considered in these applications. Early experiments on the penetration and breakup of liquid jets in supersonic crossflow[3-7] and their ignition[8] helped to enhance understanding of the fundamental physical processes involved in the problem, but detailed modeling efforts at the time proved untractable. Among the important observations made by these early researchers is the complex shock structure that forms in association with the transverse jet (see Fig. 1). Whether laminar or turbulent, the gaseous boundary layer on the flat plate upstream of the jet separates and forms a shock that attaches itself to the dominant bow shock partially surrounding the jet. Although lateral jet spread is seen to be strongly dependent on upstream Mach number, the actual degree of jet penetration depends more strongly on the jet-to-crossflow momentum flux ratio and

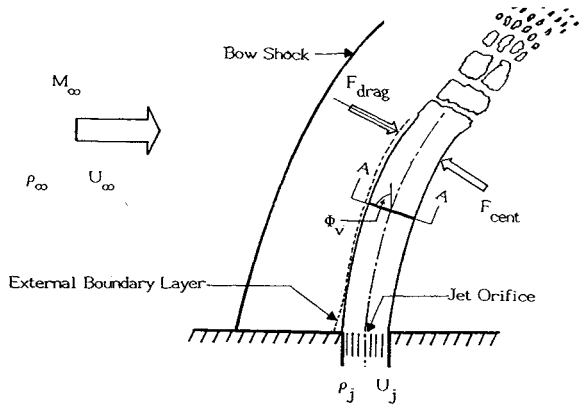

Fig. 1 Pertinent features of a single liquid jet injected into a supersonic crossflow.

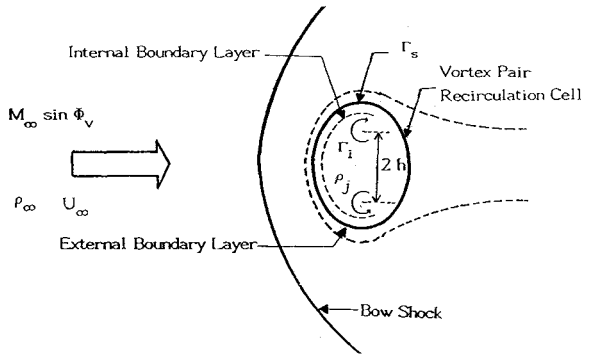

Fig. 2 Cross-sectional slice (section A-A in Fig. 1) of liquid jet in supersonic crossflow.

pressure ratio.[5] The cross section of the liquid jet is determined to deform into a characteristic horseshoe or kidney shape as a result of the pressure and shear fields present in the flowfield.[4] This type of deformed cross section is also observed to occur in jets injected transversely into crossflow of the same phase[9-11] as a result of the formation of a vortex pair structure associated with the jet cross section. This type of vortical structure also dominates the behavior of the diffusion flame in crosswind.[12-14]

More recent experimental efforts by Less and Schetz[15] indicate the importance of the jet-to-crossflow dynamic pressure ratio in predicting the structure and behavior of the liquid jet and the desirability to operate future liquid-injection systems at high dynamic pressure ratios, making use of the superior atomizing characteristics of certain liquid fuels. These researchers also note the correlation between liquid jet breakup (in both subsonic and supersonic crossflows) and the Strouhal number associated with vortices shed past a circular or elliptical surface. This observation implies a relationship between transverse liquid jet breakup and the generation of vorticity at the liquid-gas interface, which can result in the formation of vortical structures within the liquid jet and the characteristic kidney-shaped cross section.

The main purpose of the present modeling effort is to explore the nature of vorticity generation in the problem of the liquid jet injected into a compressible crossflow, and to evaluate its effect on the local drag associated with the jet cross section and, ultimately, its effect on jet penetration and bow shock shape. The influence of the upstream Mach number, the jet-to-crossflow momentum and pressure ratios, the degree of mass loss by the jet, and other features are also assessed, and the prediction of liquid jet breakup is discussed. In particular, it is desired to be able to predict liquid jet behavior without having to include empirical data in the model, as empiricism has hampered the range of applicability and fundamental nature of many of the early models.[3,7]

Description of the Model

Overall Framework

Figure 1 provides a general description of the flowfield about a liquid jet injected transversely into a supersonic gas stream. The boundary layer at the wall separates several jet diameters ahead of the injection point, thus creating a fairly low-momentum flow about the jet near the lower wall. A separation shock intersects the strong bow shock lying just ahead of the jet. The largest forces on the jet are realized in the region near the base of this bow shock, where the shock strength is greatest. The jet begins to lose structure, and breakup eventually occurs.[15] As mass is lost from the jet, large droplets are further atomized as they are swept downstream.

The present model placed emphasis on the description of the liquid jet flowfield, starting near the base of the bow shock and continuing downstream along the jet trajectory. The primary assumption employed is that jet behavior, even in its near field, may be determined by examining the dynamics of two-dimensional "slices" of the jet taken perpendicular to its centerline. An equivalent assumption has led to reasonable predictions of transverse jet behavior in low-speed crossflows of the same phase,[11,14] where the dynamics of the vortical structure associated with the jet cross section plays a critical role in determining jet trajectory and effective flame length, if a reaction is present. A crucial feature of this type of locally two-dimensional vortex modeling is that important physical processes associated with the problem must be included in representing the near field of the transverse jet. In this way the 2-D modeling, which is more appropriate further downstream, can be initiated at some downstream location with the proper "initial" conditions, ultimately yielding reasonable trajectories. Similar reasoning is employed in the present model of the liquid jet, as has been done by earlier liquid jet modelers,[3,7] although the processes of mass loss and jet breakup complicate the far-field analysis.

Figure 2 depicts the characteristic cross section of the liquid jet and the resulting external (gaseous) flowfield. The jet cross section is considered here to be composed of the elliptical recirculation cell of a vortex pair flowfield, created by pressure forces and viscous interactions between the liquid and the gaseous crossflow along the liquid-gas interface. As previously mentioned, this type of flow structure has been observed to deform the liquid jet cross section[3,4] and, as an approximation of the kidney-shaped cross section, the elliptical cross section is incorporated. As an analogy, vortical structures are also observed to form within single spherical droplets in a convective environment (the so-called Hill's spherical vortex[16]), also as a result of viscous interactions.

In taking a slice of the transverse jet as indicated in Fig. 1, the external flow approaches the jet at an effective Mach number $M = M_\infty \sin(\phi)$, where ϕ is the inclination angle perpendicular to the jet centerline, taken with respect to the vertical. By computing the pressure distribution, viscous stresses, and boundary-layer behavior at the liquid-gas interface shown in Fig. 2, the local drag associated with the jet cross section may be found. Then by employing a suitable mass and momentum balance along the jet and perpendicular to the jet to determine the relationship between flow angle ϕ, vortex half-spacing h, and the position of the cross section in the flowfield, one may ascertain the dynamic behavior of the jet including its trajectory, bow shock shape, and the local degree of mass loss due to droplet shedding.

External Flowfield Solution

The scheme developed by Godunov et al.[17] is selected to compute the inviscid flow external to the liquid jet cross section and boundary layer (Fig. 2) because of its inherent stability, its computational efficiency, and the fact that it performs well in domains where only a single shock is present. The scheme provides a first-order-accurate, explicit formula

tion of the 2-D Euler equations of gas dynamics written in conservation form.

The numerical code is constructed in finite-volume form and is able to accommodate arbitrary 2-D skewed cells. The boundary of the jet cross section is assumed to be an ellipse, so that elliptic coordinates (*ETA,PSI*) can be used to generate the grid. The assumption that the stagnation streamline for a vortex pair recirculation cell is very nearly elliptical is easily demonstrable. Figure 3 demonstrates the algebraic transformation employed to generate the computational grid. The variables *ETA* (length) and *PSI* (angle) in the transformed plane are defined

$$ETA = j/(NPTSY - 1), \qquad j = 0,(NPTSY - 1) \tag{1a}$$

$$PSI = i/NPTSX, \qquad i = 1, NPTSX \tag{1b}$$

where *NPTSX* and *NPTSY* represent the number of points encompassing the jet and the number of layers in the grid, respectively. Using elliptic coordinates, the physical variables (X, Y) can be related to *PSI* and *ETA* through the relations

$$X = \text{FOC}L \sinh[ETA\,(ETAM - ETAB) + ETAB] \sin(2\pi PSI) \tag{2a}$$

$$Y = \text{FOC}L \cosh[ETA\,(ETAM - ETAB) + ETAB] \cos(2\pi PSI) \tag{2b}$$

where FOC*L* is the ellipse focal length

$$\text{FOC}L = (YO^2 - XO^2)^{1/2}$$

and where *XO* and *YO* represent the semiminor and semimajor axes of the ellipse. The value of *ETA* at the boundary of the jet *ETAB* can also be related to the ellipse geometry:

$$ETAB = \text{arctanh}(XO/YO) \tag{3}$$

and the value of *ETA* at the outer boundary, *ETAM*, is an initial input that sets the outer limit of the computational domain. Equations (1-3) are used to generate an appropriate grid for the 2-D jet flowfield.

Results of computations on a grid in which $XO = 1.73$, $YO = 2.09$, and $ETAM = 4.0$ (*ETAB*) are provided in Figs. 4-6. Figure 4 details bow shock position for three different upstream Mach numbers. The bow shock structure is actually slightly smeared here, due to the numerical technique, over three to four computational cells. It should be noted that when the elliptical surface is reduced very nearly to a circle, the bow shock shape predicted by the present code corresponds very closely to the earlier numerical results obtained by Belotserkovskii.[18] Figures 5 and 6 describe the variation in velocity components, and pressure and density, respectively, along the surface of the ellipse, starting at the stagnation point. As the flow decelerates beyond the shoulder of the ellipse, a sharp drop in velocity (and an increase in static pressure) are observed to occur along the ellipse, indicating the presence of attached shocks adjacent to the cross section of the liquid jet. The formation of these shocks will be used to predict external boundary-layer separation, described in the next section. It should be noted that the Godunov scheme is also applicable to the case of high subsonic upstream flows, and the present code has been run in this flow regime with similar success. Hence, this numerical procedure may be applied to determine flow solutions at the jet boundary for the entire range of Mach numbers encountered along the jet.

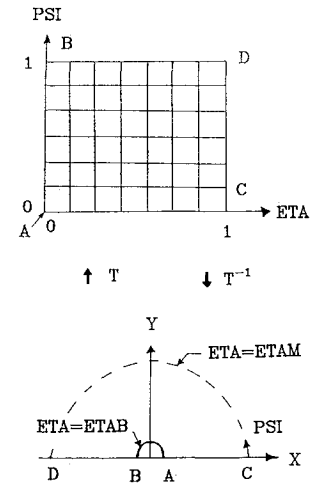

Fig. 3 Description of grid generation scheme for elliptical computational cells.

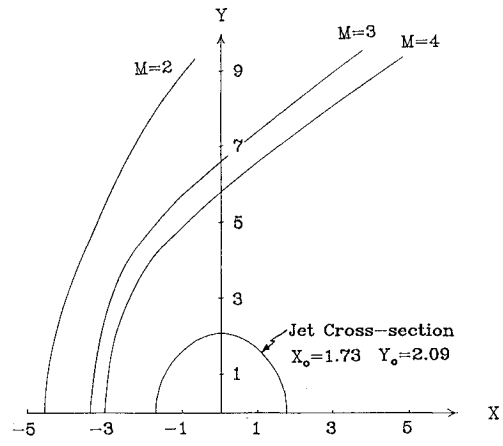

Fig. 4 Computed shapes of bow shocks formed ahead of elliptical cross section for different Mach numbers.

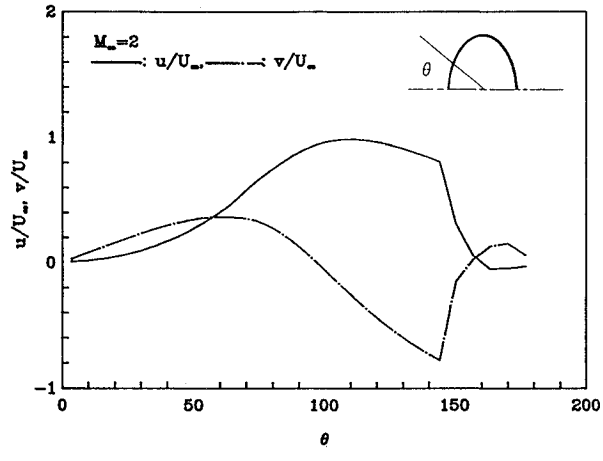

Fig. 5 Computed velocity components along surface of elliptical cross section for upstream Mach number $M_\infty = 2.0$.

Internal Flowfield and Jet Dynamics Model

Use of the numerical procedure described above allows calculation of the shape and standoff distance of the bow shock in the plane of the jet's cross section in addition to properties behind the shock and along the surface of the ellipse. The exact correspondence of the angle of jet orientation ϕ to the actual location of the jet cross section in the flowfield, however, must be determined. Once this is accomplished, the predicted shape of the bow shock and jet trajectory in the plane of the transverse jet (as shown in Fig. 1) may

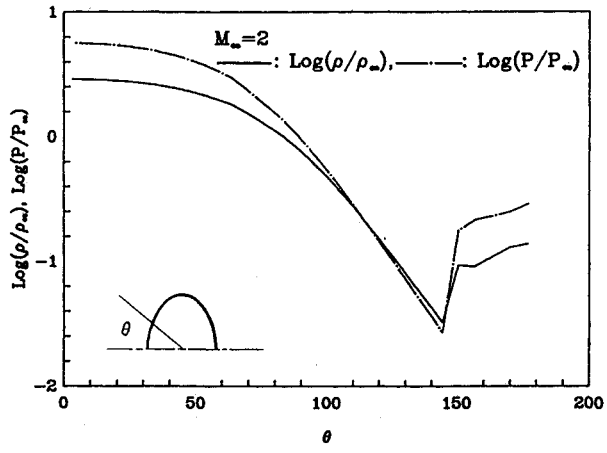

Fig. 6 Computed density and pressure ratios along surface of elliptical cross section for upstream Mach number $M_\infty = 2.0$.

be obtained. This correspondence is achieved by application of a force balance in the plane of the jet cross section, and by solution of the equations of mass and momentum conservation applied along the jet trajectory. A preliminary assumption made in the present analysis is that evaporation of the liquid at the interface can be neglected; later studies will include this effect.

The reference frame for evaluation of the force balance normal to the jet is shown in Fig. 1. Here the drag acting on the elliptical cross section of the jet (due to aerodynamic and viscous effects) must balance the centripetal forces acting as a result of jet deflection. The drag here is computed by incorporating the inviscid flow solution about the ellipse as the "outer flowfield" seen by external (gaseous) boundary layer of the jet cross section. Calculation of the growth of the external boundary layer and determination of the local shear stress acting along the liquid-gas interface is performed using the approximate integral techniques of Gruschwitz[19] and Flügge-Lotz and Johnson[20] for compressible boundary layers. The Gruschwitz solution, which employs a fourth-order polynomial to approximate flow in a gaseous boundary layer, is used from the stagnation point to the shoulder (top) of the ellipse, while the Flügge-Lotz and Johnson solution (employing a fifth-order polynomial) is used from the shoulder to the point of separation. The dual methods are employed here because of the superior ability of the fifth-order polynomial solution to predict separation.[20]

The present situation is complicated by the fact that the velocity of the liquid at the interface is nonzero, since the external (gaseous) flow drives the internal (liquid) flow within the jet cross section. Details of the flowfield are described in Fig. 2. Because of the nonzero surface velocity U_s in the present case, the fourth-order polynomial used to characterize the flow in the external boundary layer (between the stagnation point and the shoulder) takes the form

$$\frac{u_{o1}(x,y)}{U_o} = f_1(\eta) = F_1(\eta) + \lambda_1 G_1(\eta) + \frac{U_s}{U_o} \tag{4}$$

where

$$F_1(\eta) = \left(1 - \frac{U_s}{U_o}\right)(2\eta - 2\eta^3 + \eta^4)$$

$$G_1(\eta) = \frac{\eta\,(1-\eta)^3}{6}$$

$$\eta \equiv \frac{1}{\delta'}\int_o^y \frac{\rho}{\rho_o}\,d\hat{y}, \qquad \delta'(x) = \int_o^\delta \frac{\rho}{\rho_o}\,d\hat{y}$$

and

$$\lambda_1(x) = \left(\frac{\rho_o}{\rho_s}\right)^2 \frac{\delta'^2}{\nu_s}\left[\frac{dU_o}{dx}\right]\left[1 - \left(\frac{U_s}{U_o}\right)^2\right]$$

Here the subscript o refers to flow conditions outside of the external boundary layer, and the subscript s refers to surface conditions. The fifth-order plynomial used to characterize external boundary-layer flow between the shoulder and sepration point takes the form

$$\frac{u_{o2}(x,y)}{U_o} = \frac{[1-(U_s/U_0)]}{\lambda+18} F_2(\eta) + \frac{\lambda_2}{\lambda+18} G_2(\eta) + \frac{U_s}{U_o} \tag{5}$$

where

$$F_2(\eta) = 30\eta + 10\lambda\eta^3 - 15\,(\lambda+2)\,\eta^4 + 6\,(\lambda+3)\,\eta^5$$

$$G_2(\eta) = \frac{9}{2}\eta - \frac{1}{2}(\lambda+18)\,\eta^2 + \frac{3}{2}\lambda\eta^3 + \frac{3}{2}(6-\lambda)\,\eta^4 + \frac{1}{2}(\lambda-9)\,\eta^5$$

and

$$\lambda(x) = \left(\frac{\rho_o}{\rho_s}\right)^2 \frac{\delta'^2}{\nu_s}\left(\frac{U_s}{U_o}\right)\frac{dU_o}{dx}$$

$$\lambda_2(x) = \frac{[1-(U_s/U_o)^2]}{U_s/U_o}\,\lambda(x)$$

Because the cross section of the liquid jet is represented by an elliptical vortex pair recirculation cell, characterization of the surface velocity U_s can be made in terms of an effective dimensionless circulation Γ_s:

$$\frac{U_s}{U_\infty} = \Gamma_s \frac{U_o}{U_\infty} \tag{6}$$

where U_o is the local velocity external to the boundary layer, determined from the inviscid numerical solution, and U_∞ is the freestream velocity.

The governing equation for the external boundary layer, derived from the momentum integral equation, is consistent with the aforementioned integral methods at unity Prandtl number. This equation takes the form

$$\frac{d\tilde{\delta}_2}{d\tilde{x}} + [(2-M_o^2)\,\tilde{\delta}_2 + \tilde{\delta}_1]\,\frac{1}{\tilde{U}_o}\frac{d\tilde{U}_o}{d\tilde{x}}\left(\frac{\tilde{\nu}_o}{\tilde{\delta}'Re_\infty}\right)\frac{1}{\tilde{U}_o}\left(2 + \frac{\lambda_i}{6} - 2\Gamma_s\right) \tag{7}$$

where

$$\tilde{\delta}_1 \equiv \frac{\delta_1}{h} = \frac{1}{h}\int_o^\delta \left[1 - \frac{\rho u_{oi}}{\rho_o U_o}\right] dy \tag{8}$$

and

$$\tilde{\delta}_2 \equiv \frac{\delta_2}{h} = \frac{1}{h}\int_o^\delta \frac{\rho u_{oi}}{\rho_o U_o}\left[1 - \frac{u_{oi}}{U_o}\right] dy \tag{9}$$

are the dimensionless displacement and momentum thicknesses, respectively. The subscript i in relations (7-9) corresponds to the fourth-order ($i = 1$) or fifth-order ($i = 2$) solutions where appropriate. These and other length parameters in the problem are nondimensionalized by h, the characteristic vortex pair half-spacing. Other parameters (e.g., $\tilde{\rho}_o$, $\tilde{U}_o$, etc.) represent quantities that have been nondimensionalized by conditions at upstream infinity.

It should be noted that, in a manner similar to that of the classical compressible laminar boundary-layer solutions, an adiabatic wall condition is employed in the above analysis. It is also of interest to note that if there were no surface flow (i.e., $\Gamma_s = 0$), the above equations reduce to the integral equations for the Gruschwitz and Flügge-Lotz-Johnson solutions. When ideal gas relations are employed, the polynomial expressions for the velocity profile in the layer are incorporated, as appropriate, and the "outer flow" solution is introduced from the inviscid numerical procedure. The governing equation (9) is then solved numerically along the surface of the ellipse or jet cross section as long as a solution for the effective surface circulation Γ_s is known.

Solution of the effective surface circulation Γ_s is obtained in a straightforward manner by solving the governing equation at the stagnation point of the ellipse. This yields a single polynomial equation for the possible solutions of Γ_s. The stagnation point solution appropriate to the present problem is

$$\Gamma_s = 0.1234 \tag{10}$$

and

$$\lambda_{1(\text{stag})} = 7.052\ (1 - \Gamma_s^2) \tag{11}$$

It is again noted that if Γ_s were equal to zero, the solution for the boundary-layer parameter λ_1 at the stagnation point reduces to that found in the classic compressible boundary-layer solution.

Now that both Γ_s and the stagnation point solution are known, the outer flow result is used so that Eq. (9) may be solved numerically (via backward differencing) along the surface of the ellipse. Typical solutions for the variation in displacement thickness along the jet cross section are shown in Fig. 7 for different upstream Mach numbers. As is appropriate, the higher upstream Mach number reduces the displacement thickness of the gas boundary layers and, to a minor extent, delays separation of the boundary layer. Another pertinent parameter that may be obtained from this solution is the local shear stress τ_s acting at the liquid-gas interface, so that the point of separation in the rearward portion of the ellipse may be determined. In the situations where the Godunov solution predicts the formation of a locally normal shock attached to the rearward portion of the ellipse (typically for $M_\infty > 0.8$), separation is assumed to occur very nearly at the point of shock attachment, even if the local shear stress has not yet gone through zero.

An effective drag coefficient C_D associated with the jet cross section is now found by integration of the local shear stress and the numerically computed pressure distribution along the liquid-gas interface. It is assumed that beyond the separation point the pressure acting at the surface is averaged between the computed pressures at the separation and rearward stagnation points, a method shown to be reasonable by Gonor.[21] Hence, for different upstream conditions (e.g., Mach number) seen by the local jet cross section, an approximate drag coefficient for the elliptical cross section may be computed according to the above procedure. Results from this computation are shown as a function of Mach number in Fig. 8. This figure also indicates the variation in drag coefficient on a cylinder obtained from an empirical correlation; it is this correlation that has been used to represent drag on the jet cross section in earlier transverse jet models.[7] The figure also indicates the effect of setting the surface velocity of the ellipse or the cylinder equal to zero (i.e., $\Gamma_s = 0$), and the effect of ignoring the surface shear stress τ_s on calculation of the drag coefficient. It is clear from Fig. 8 that 1) if the present calculation scheme is performed for compressible flow over a cylinder (with no surface flow), there is excellent correspondence between our calculation and the empirical correlation, especially for supersonic crossflow, 2) for the present calculation, inclusion of liquid surface flow (via U_s or Γ_s) and the presence of the external boundary layer (via τ_s) make little difference in the calculation of drag on the ellipse, and 3) because of the differences in drag coefficient associated with a cylinder and an ellipse, the present calculation applied to the ellipse is considered to be superior to earlier transverse jet models in that a more realistic approximation for the kidney-shaped jet cross section is employed.

Based on this determination of the drag coefficient C_D, the force balance perpendicular to the jet trajectory may be performed. The resulting governing equation for ϕ, the angle of orientation of the local jet cross section, takes the form

$$\frac{d\phi}{ds} = \left[-2C_D\left(\frac{a}{b}\right)^{1/2} \sin^2\phi \right] / (\pi R u_j^{3/2}) \tag{12}$$

where R^2 is the jet-to-crossflow momentum flux ratio $\rho_j U_j^2 / \rho_\infty U_\infty^2$, u_j is the average axial velocity within the jet, and a and b are the semimajor and semiminor axes of the ellipse, approximately equal to $2.09h$ and $1.73h$, respectively. It should be noted that Eq. (12) cannot be solved along the jet trajectory, because the local (mass-averaged) axial velocity within the jet, u_j, is yet unknown.

A combination of mass and momentum conservation equations in the plane of the jet trajectory yields an ordinary

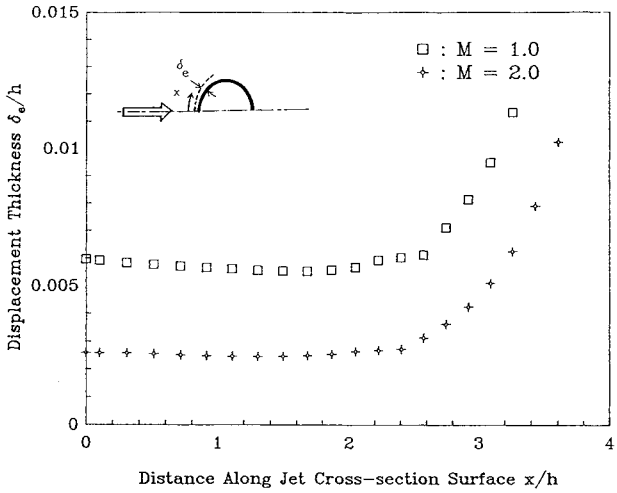

Fig. 7 Computed variation in displacement thickness of external boundary layer with distance along surface of elliptical cross section.

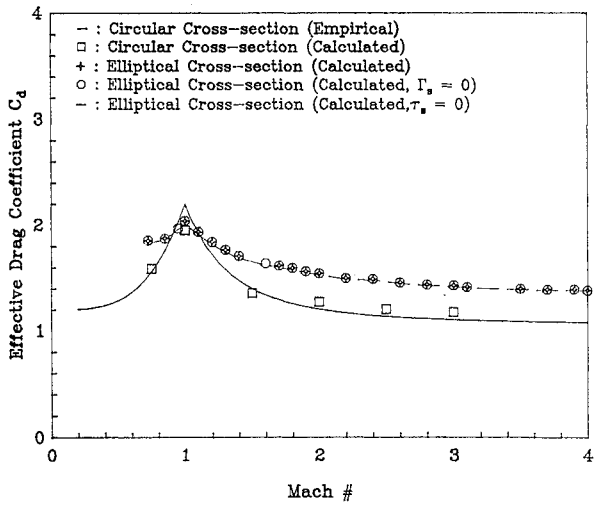

Fig. 8 Computed variation in drag coefficient C_D with upstream Mach number for elliptical cross section (with surface flow and viscous stresses (+), with $\Gamma_s = 0$ (o), and with $\tau = 0$).

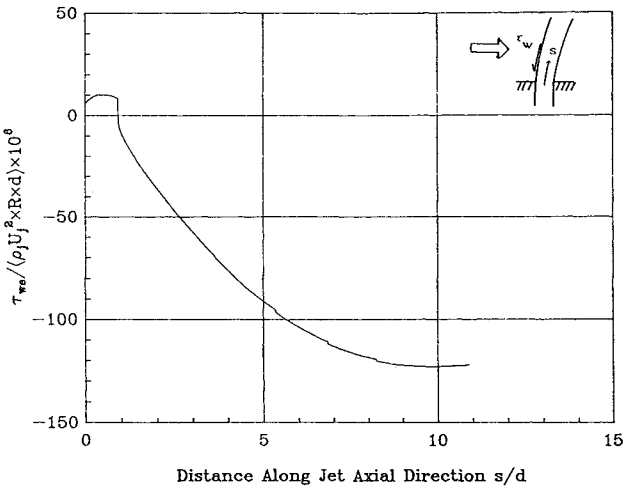

Fig. 9 Computed variation in external shear stress (measured at forward stagnation point) along the jet trajectory for upstream Mach number $M_\infty = 2.0$, $R = 2.5$, and $Re_\infty = 10^5$.

differential equation in the local mass-averaged axial velocity in the jet, u_j, and the dimensions of the elliptical cross section:

$$\frac{d(mu_j)}{ds} = \frac{-\tau_{w,e}\pi(a+b)}{2} - A\frac{dP}{ds} \tag{13}$$

where $\tau_{w,e}$ is the external shear stress acting at the stagnation point along the jet trajectory (computed again by the Gruschwitz or Flügge-Lotz-Johnson methods), and A is the cross-sectional area of the jet slice. Typical results for the variation in external shear stress are shown in Fig. 9. Because the liquid axial velocity at the jet orifice is of greater magnitude than the local component of gas flow outside of the jet, the shear stress starts out as positive, but as the jet turns, the component of gas velocity increases, and shear stess goes through zero and becomes negative for the majority of the jet trajectory. The magnitude of the shear stress appears to level off at approximately 10 jet diameters along the trajectory, which coincides under some circumstances with complete liquid jet breakup.

With initial conditions corresponding to the velocity and size of the jet at the orifice, Eqs. (13) and (12) may now be solved simultaneouly to yield a correspondence between flow angle ϕ, axial velocity u_j, and distance along the trajectory. This information may be used to determine the orientation and location of the local jet cross sections analyzed and, hence, calculation of preliminary trajectories of the liquid jet and bow shock is possible.

The procedure described above for the momentum calculation performed along the jet does not, as shown, account for the loss of mass that occurs due to the shearing off of droplets from the jet. A simple methodology that can be used to estimate mass along the jet incorporates an evaluation of the local internal (liquid) boundary layer at each cross-sectional slice of the liquid jet, and considers that the fluid in the internal boundary layer is continually shed from the jet as one moves downstream along the trajectory. This approach is modeled after the technique utilized by Korner[22] for mass loss in a liquid droplet, but evaluates the internal boundary layer by the approximate technique of Pohlhausen, as described previously for the external boundary layer, with a fourth-order polynomial representing the flow in the liquid boundary layer. The expression in Eq. (4) is again appropriate, except that U_o is replaced by an effective "freestream" velocity within the liquid, U_i. Since the incompressible flowfield within the liquid cross section is assumed to be that within a vortex pair recirculation cell, the velocity field U_i may be represented in terms of an internal circulation Γ_i, so that $\tilde{U}_i = \Gamma_i \tilde{U}_o$. Solution of the governing Eq. (4) at the stagnation point of the ellipse yields an approximation for Γ_i as 0.035. From this evaluation, the governing momentum integral equation may be solved numerically along the elliptical surface, providing solutions for the variation in displacement and momentum thicknesses and shear stress within the liquid.

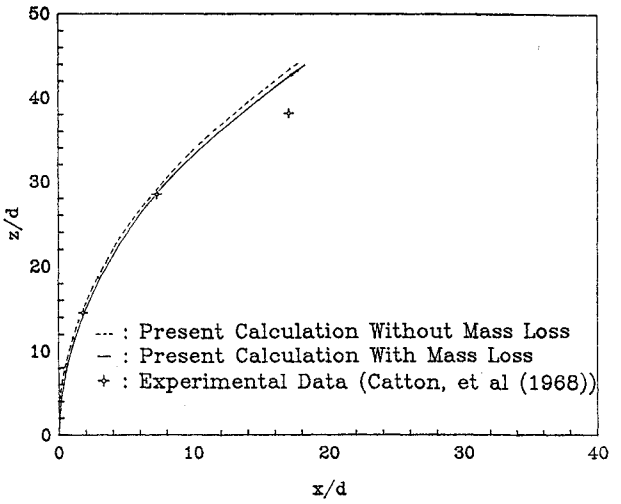

Fig. 10a Computed jet trajectory for $M_\infty = 4.1$, $R = 7.7$ (with and without mass loss) compared with experimental results.

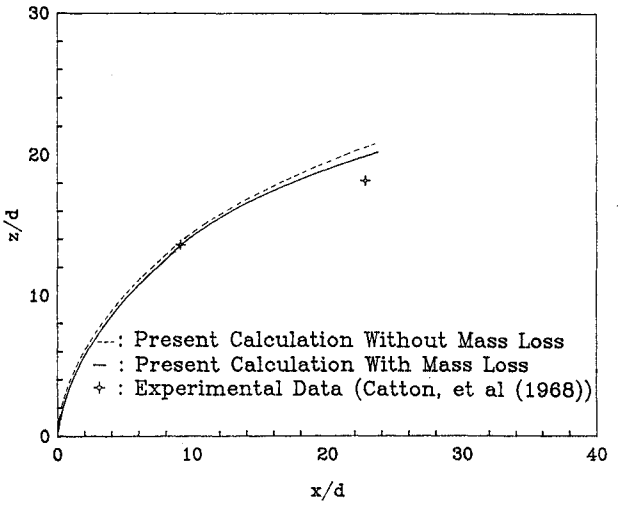

Fig. 10b Computed jet trajectory for $M_\infty = 4.1$, $R = 2.6$ (with and without mass loss) compared with experimental results.

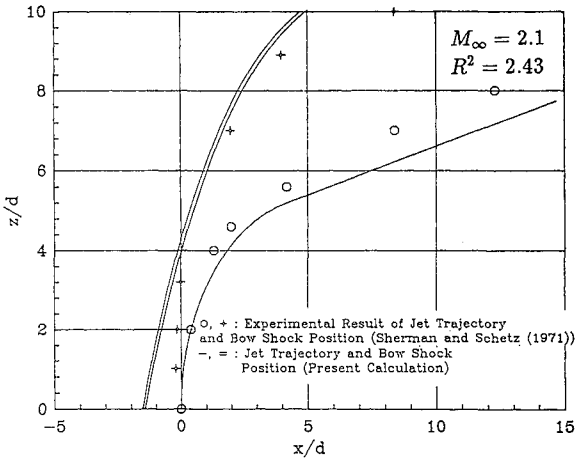

Fig. 11 Computed jet trajectory and bow shock shape for $M_\infty = 2.1$, $R = 2.43$ (with and without mass loss) compared with experimental results.

In accordance with the methodology of Korner,[22] the displacement thickness of the interal flow at the point of external boundary-layer separation is used to approximate the mass flux of liquid lost at a given cross-sectional slice of the jet. This assumption is consistent with phenomena that are observed in experiments to contribute to droplet shedding from circular and elliptical surfaces. The rate at which mass is lost from a section of the jet trajectory of length ds then can be expressed as

$$\dot{m} = 2ds\int_o^{\delta_{il}} \rho_i U_i\left(\frac{u_i}{U_i}\right) dy = 2ds\,(\rho_i\delta_i U_i)\left[\frac{\lambda_i}{120}+\frac{7}{10}+\frac{3}{10}\frac{\Gamma_s}{\Gamma_i}\right] \tag{14}$$

where the subscript i is used to denote boundary layer and flow quantities within the liquid. This mass loss can now be considered in the momentum balance along the jet, modifying Eq. (13) to take the form

$$\frac{du_j}{ds} = \frac{2}{A}\left[(\delta_i U_i)\left(\frac{\lambda_i}{120}+\frac{7}{10}+\frac{3}{10}\frac{\Gamma_s}{\Gamma_i}\right)\right] - \frac{2\tau_{s,e}x_s}{\rho_i U_j A} - \frac{1}{\rho_j U_j}\frac{dP}{ds} \tag{15}$$

where $\tau_{s,e}$ is the external shear stress at the separation point, x_s is the location (along the surface of the jet cross section) of separation, and A, the instantaneous cross-sectional area of the jet, is found by mass conservation along the jet to satisfy the equation

$$\frac{dA}{ds} = \frac{-2}{u_j}\left[\delta_i U_i\left(\frac{\lambda_i}{120}+\frac{7}{10}+\frac{3}{10}\frac{\Gamma_s}{\Gamma_i}\right)\right] - \frac{A}{u_j}\frac{du_j}{ds} \tag{16}$$

Hence, simultaneous solution of the momentum and mass conservation equations above [Eqs. (15) and (16), respectively], in conjunction with the force balance in the plane of the jet cross section [Eq. (12)], allows for a modified jet trajectory to be obtained in which we have accounted for the loss of mass due to droplet shedding.

Results and Conclusions

Determination of the jet trajectory by the two methods outlined above can be made, one without mass loss and the other with mass loss included, as can comparison of trajectory results with the limited experimental data that are available. These comparisons are shown in Fig. 10 for various values of the upstream Mach number M_∞ and the jet-to-crossflow momentum flux ratio R^2. Clearly, representation of mass loss in the present model does not strongly alter the degree of jet penetration predicted, although closer approximations to experimental data are obtained when mass loss is included. It should be noted that the relative importance of mass loss for the actual liquid jet in crossflow is likely to be greater than in the present vortex model, in that the actual cross-sectional area of the jet is distorted from its elliptical or, actually, kidney shape, due to surface waves. The overall ability of the present model to predict jet trajectories, however, is quite good within 10–15 jet diameters downstream of injection. Beyond this point, most liquid transverse jets have broken up completely, and our model is no longer applicable in its present form.

Although data corresponding to both jet trajectory and bow shock position are even more scarce then those corresponding to trajectories only, measurements of shock location made from photographs in a paper by Sherman and Schetz[23] can be compared with predictions by the present model and are shown in Fig. 11. Again, somewhat superior correlation is obtained when mass loss is taken into account. The predicted bow shock position agrees quite well with the data, considering the nature of the assumptions that have been made (e.g., neglect of the wall boundary layer) and the approximate nature of the experimental data. The jet trajectory is also in good agreement with the data, as the experimental data points shown represent the top of the liquid jet, while the predictions apply for the jet centerline.

The results indicate that most of the features of the present analytical/numerical model accurately represent the important flow processes for a liquid jet injected into a supersonic crossflow. In particular, the novel approach taken here in characterizing the jet cross section as an elliptical vortex pair recirculation cell, rather than as a simple circular cross section,[3,7] seems to produce superior results (in terms of predicted jet and shock trajectories) without the use of any empirical data. The incorporation of empirical correlations considerably reduces the range of applicability of prior modeling efforts. Although a more accurate description of the local drag coefficient associated with the jet cross section is obtained here at supersonic conditions, the subonic formulation (see Fig. 8) becomes less accurate below Mach number $M_\infty = 0.6$. This is because the numerical procedure of Godunov is not as accurate at lower subsonic Mach numbers, and introduces errors into the evaluation of drag coefficient in this regime.

Of course, further downstream, beyond 10 jet diameters, it is likely that complete jet breakup has occured, so that the collective drag coefficient of the liquid droplets in the jet vicinity is actually higher than that predicted by the present model. Experimental results shown by Adelberg[7] and Sherman and Schetz[23] demonstrate that it is difficult to describe the jet breakup location, since the coherence of the jet is rather unclear in this region anyway. Although our prediction of a maximum in the external shear stress along the jet at roughly 10 jet diameters could mean that a maximum in destabilizing forces is adequate to predict breakup, the physics of the breakup phenomenon is more complicated than can be represented by the present vortex model. To date, there are no papers available that describe experimentally observed breakup locations for the liquid transverse jet. More detailed study is required to describe this highly complex flow process.

In addition to the exploration of breakup processes, future studies will concentrate on prediction of liquid transverse jet behavior in low-to-moderate subsonic crossflows, a flow regime that is not accurately modeled by the present Godunov procedure. Future analyses will also explore the effect of evaporation at the liquid surface (expected to be small) and the effect of nonuniform initial conditions for the liquid jet due to wall boundary-layer separation and shock formation ahead of injection.

Acknowledgments

The authors wish to acknowledge the support of the U.S. Department of Energy under Grant DE-FG03-88-ER13910 and NASA Ames/Dryden Research Center under Grant NCC 2-374, in addition to helpful discussions with Dr. James McDonough of the University of California, Los Angeles.

References

[1]Reider, S. B., "Air Breathing Propulsion—Aerospace Highlights 1986," *Aerospace America*, Vol. 24, No. 12, 1986, pp. 32–33.

[2]"Propelling the Aerospace Plane," *Mechanical Engineering*, ASME Staff Rept., Vol. 108, Jan. 1986, pp. 32–37.

[3]Catton, I., Hill, D. E., and McRae, R. P., "Study of Liquid Jet Penetration in a Hypersonic Stream," *AIAA Journal*, Vol. 6, No. 11, 1968, pp. 2084–2089.

[4]Forde, J. M., Molder, S., and Szpiro, E. J., "Secondary Liquid Injection into a Supersonic Airstream," *Journal of Spacecraft and Rockets*, Vol. 3, No. 8, 1966, pp. 1172–1176.

[5]Kolpin, M. A., Horn, K. P., and Reichenback, R. E., "Study of Penetration of a Liquid Injectant into a Supersonic Flow," *AIAA Journal*, Vol. 6, No. 5, 1968, pp. 853–858.

[6]Horn, K. P. and Reichenbach, R. E., "Further Experiments on Spreading of Liquids Injected into Supersonic Flow," *AIAA Journal*, Vol. 7, No. 2, 1969, pp. 38–39.

[7]Adelberg, M., "Breakup Rate and Penetration of a Liquid Jet in a Gas Stream," *AIAA Journal*, Vol. 5, No. 8, 1967, pp. 1408–1415.

[8]Schetz, J. A. and Cannon, S. C., "Ignition of Liquid Fuels in Supersonic Air Streams," Virginia Polytechnic Institute and State University, AFOSR-TR-78-1098, May 1978.

[9]Kamotani, Y. and Greber, I., "Experiments on a Turbulent Jet in a Cross Flow," *AIAA Journal*, Vol. 10, No. 11, 1972, pp. 1425–1429.

[10]Fearn, R. and Weston, R. P., "Vorticity Associated with a Transverse Jet," *AIAA Journal*, Vol. 12, No. 12, 1974, pp. 1666–1671.

[11]Karagozian, A. R., "An Analytical Model for the Vorticity Associated with a Transverse Jet," *AIAA Journal*, Vol. 24, No. 3, 1986, pp. 429–436.

[12]Brzustowski, T. A., "Flaring in the Energy Industry," *Progress in Energy and Combustion Science*, Vol. 2, No. 3, 1976, pp. 129–141.

[13]Broadwell, J. E. and Breidenthal, R. E., "Structural and Mixing of a Transverse Jet in Incompressible Flow," *Journal of Fluid Mechanics*, Vol. 148, 1984, pp. 405–412.

[14]Karagozian, A. R., "The Flame Structure and Vorticity Generated by a Chemically Reacting Transverse Jet," *AIAA Journal*, Vol. 24, No. 9, 1986, pp. 1502–1507.

[15]Less, D. M. and Schetz, J. A., "Transient Behavior of Liquid Jets Injected Normal to a High-Velocity Gas Stream," *AIAA Journal*, Vol. 24, No. 12, 1986, pp. 1979–1986.

[16]Clift, R., Grace, J. R., and Weber, M. E., *Bubbles, Drops, and Particles*, Academic Press, New York, 1978.

[17]Godunov, S. K., Zabrodin, A. V., and Prokopov, G. P., "A Computational Scheme for Two-Dimensional Non-Stationary Problems of Gas Dynamics and Calculation of the Flow from a Shock Wave Approaching a Steady State," *USSR Computational Mathematics and Math Physics*, May 1961.

[18]Belotserkovskii, O. M., "Flow Past a Circular Cylinder with a Detached Shock Wave," translated as RAD-9-TM-59-66, Avco Corp., Research and Advanced Development Division, 1959.

[19]Gruschwitz, E., "Calcul approché de la couche limite laminaire en écoulement compressible sur une paroi non-conductrice de la chaleur," ONERA Pub 47, Paris, 1950.

[20]Flügge-Lotz, I. and Johnson, A. F., "Laminar Compressible Boundary Layer Along a Curved Insulated Surface," *Journal of the Aeronautical Sciences*, Vol. 22, No. 7, 1955, pp. 445–454.

[21]Gonor, A. L., "Motion and Deformation of a Drop in a Gas Flow," *Fluid Mechnics—Soviet Research*, Vol. 9, No. 1, 1980, pp. 21–38.

[22]Korner, W., "The Behaviour of Drops in High Velocity Gas Jets," Royal Aircraft Establishment, N75-11212, Great Britain, June 1974.

[23]Sherman, A. and Schetz, J., "Liquid Sheets and Liquid Jets in a Supersonic Stream," *AIAA Journal*, Vol. 9, No. 4, 1971, p. 666.